Alterations in Protein Regulators of Neurodevelopment in the Cerebrospinal Fluid of Infants with Posthemorrhagic Hydrocephalus of Prematurity*[S]

Diego M. Morales‡, R. Reid Townsend§¶, James P. Malone§, Carissa A. Ewersmann‡, Elizabeth M. Macy§, Terrie E. Inder‖, and David D. Limbrick Jr.‡‖**

Neurological outcomes of preterm infants with posthemorrhagic hydrocephalus are among the worst in newborn medicine. There remains no consensus regarding the diagnosis or treatment of posthemorrhagic hydrocephalus, and the pathological pathways leading to the adverse neurological sequelae are poorly understood. In the current study, we developed an innovative approach to simultaneously identify potential diagnostic markers of posthemorrhagic hydrocephalus and investigate novel pathways of posthemorrhagic hydrocephalus-related neurological disability. Tandem multi-affinity fractionation for specific removal of plasma proteins from the hemorrhagic cerebrospinal fluid samples was combined with high resolution label-free quantitative proteomics. Analysis of cerebrospinal fluid obtained from infants with posthemorrhagic hydrocephalus demonstrated marked differences in the levels of 438 proteins when compared with cerebrospinal fluid from age-matched control infants. Amyloid precursor protein, neural cell adhesion molecule-L1, neural cell adhesion molecule-1, brevican and other proteins with important roles in neurodevelopment showed profound elevations in posthemorrhagic hydrocephalus cerebrospinal fluid compared with control. Initiation of neurosurgical treatment of posthemorrhagic hydrocephalus resulted in resolution of these elevations. The results from this foundational study demonstrate the significant promise of tandem multi-affinity fractionation-proteomics in the identification and quantitation of protein mediators of neurodevelopment and neurological injury. More specifically, our results suggest that cerebrospinal fluid levels of proteins such as amyloid precursor protein or neural cell adhesion molecule-L1 should be investigated as potential diagnostic markers of posthemorrhagic hydrocephalus. Notably, dysregulation of the levels these and other proteins may directly affect ongoing neurodevelopmental processes in these preterm infants, providing an entirely new hypothesis for the developmental disability associated with posthemorrhagic hydrocephalus. ***Molecular & Cellular Proteomics 11: 10.1074/mcp.M111.011973, 1–15, 2012.***

Intraventricular hemorrhage (IVH)[1] remains a common and severe neurological complication of preterm birth, occurring in roughly 25% of very low birth weight infants (1). Posthemorrhagic hydrocephalus (PHH) occurs in up to one half of infants with IVH and is associated with a 3–4 fold increase in the risk of cognitive and psychomotor disability. Infants with PHH who require ventriculoperitoneal (VP) shunts suffer the worst neurological outcomes with neurodevelopmental impairments observed in $>$ 85% of infants and cerebral palsy in nearly 70% (2). Despite its profound effects on neurodevelopment, there remains no consensus regarding the diagnosis or treatment of PHH. Current clinical and radiographic tools used in the evaluation of PHH are crude and often result in delays in the identification of infants who need surgery to prevent further irreversible neurological injury. The lack of definitive diagnostic tools for PHH also has contributed to tremendous variability in clinical practice

From the Departments of ‡Neurological Surgery, §Medicine, ¶Cell Biology and Physiology, and ‖Pediatrics. Washington University in Saint Louis School of Medicine, Saint Louis, Missouri 63110

Received June 17, 2011, and in revised form, November 18, 2011
Published, MCP Papers in Press, December 20, 2011, DOI 10.1074/mcp.M111.011973

[1] The abbreviations used are: ActB, beta actin; ADAM10, disintegrin and metalloprotease 10; ApoA2, apolipoprotein II; ApoA4, apolipoprotein IV; APP, amyloid precursor protein; BCAN, brevican; CHGA, Chromagranin A; CLSTN1, calsyntenin-1; CSF, cerebrospinal fluid; CV, coefficients of variation; ECM, extracellular matrix; EGA, estimated gestational age; HRP, horseradish peroxidase; ID, immunodepleted; IPA, Ingenuity Pathway Analysis; IS, initial sample; IVH, intraventricular hemorrhage; LC-MS, nano-liquid chromatography interfaced to high resolution mass spectrometry; L1CAM, neural cell adhesion molecule-L1; LP, lumbar puncture; LY6H, lymphocyte antigen 6H; MAF, multi-affinity fractionation; MMP9, matrix metalloproteinase-9; NCAM-1, neural cell adhesion molecule-1; NCAN, neurocan core protein; NICU, neonatal intensive care unit; PHH, posthemorrhagic hydrocephalus; SERPINF1, pigment epithelium-derived factor; TBST, tris-buffered saline – tween20; TEA, term-equivalent age; VP, ventriculoperitoneal.

and has hamstrung efforts to improve the outcomes of this condition.

PHH typically occurs in preterm infants between 24 and 40 weeks estimated gestational age (EGA). This period is crucial for central nervous system development, with ongoing neurogenesis, precursor differentiation and migration, synaptogenesis, myelination, and cortical folding. Also during this interval, functional neural networks are established in parallel with the development and maturation of cortical architecture and white matter tracts (3). Recent research has focused on the interplay between cerebrospinal fluid (CSF) signals and their role in normal neurodevelopment (4), and there is growing evidence that secreted proteins or other factors within the CSF have an age-dependent effect on neural precursor proliferation and cortical development (5). Thus, major alterations in the CSF protein landscape in neonatal neurological disease states such as PHH could have pervasive effects on global neurodevelopment.

Discovery-oriented technologies such as proteomics have been increasingly employed to examine CSF for markers of neurological disease. Although proteomics has been applied to a small, heterogenous cohort of CSF samples from individuals with hydrocephalus of various types (6), this technique has never been used to study the CSF of preterm infants with PHH. An abundance of hemorrhage-related, nonspecific, or contaminant proteins in the CSF has prohibited its application in PHH. Indeed, the range of protein concentrations would be expected to be greater than 10 orders of magnitude (7). Multi-affinity fractionation (MAF) has been used in studies of plasma and CSF to remove six to14 high abundance proteins (~1–50 mg/ml) and increase the number of moderate- and low-abundance proteins that can be identified using proteomics methods (8–12). More recently, a multi-affinity method using IgY antibodies raised against depleted human plasma was developed to selectively enrich lower abundance proteins (~< 1 μg/ml) and facilitate diagnostic marker studies in plasma (13). In the current study, we tested whether a combination of both columns would enable the identification and quantification of neurodevelopmental proteins in limited quantities of CSF from preterm infants with PHH. We developed a novel platform that features serial, inline immunoaffinity depletion, high-resolution comparative liquid chromatography-mass spectrometry (LC-MS) proteomics, and a linear mixed hierarchical statistical model to quantify CSF proteins from premature infants. The application of this discovery approach in the premature infant may yield important information regarding the landscape of low-abundance proteins in the developing human brain and provide insight into PHH-related alterations in neurodevelopmental processes.

EXPERIMENTAL PROCEDURES

CSF Collection—Approval from the Washington University Human Research Protection Office (#09–0183) was acquired prior to the initiation of this study. All preterm infants < 34 weeks EGA admitted to the St. Louis Children's Hospital Neonatal Intensive Care Unit (NICU) underwent routine head ultrasound examinations between 0 and 5 days of age to screen for IVH. Those found to have IVH then had weekly ultrasounds to monitor for PHH. Requirement for implantation of a ventricular reservoir to treat PHH was at the discretion of the treating neonatologist and neurosurgeon. Once a reservoir was implanted, serial head ultrasounds and physical parameters (occipitofrontal circumference, palpation of the anterior fontanel, splaying of cranial sutures) were used to direct the timing and volume of CSF removed for ventricular decompression. As each infant approached term-equivalent age (TEA), the need for continued CSF removal was assessed and a determination was made if the infant would require a permanent VP shunt. All subjects included in this study required a VP shunt, and no additional CSF was obtained after the shunt was implanted.

For PHH CSF, the initial sample (IS) was obtained directly from the operating room at the time of initial ventricular cannulation during reservoir implantation. Additional PHH CSF samples were collected from the operating room during implantation of a VP shunt at TEA. Between IS and TEA, CSF was removed from each reservoir in the NICU under sterile conditions as clinically indicated. Control CSF was obtained by lumbar puncture (LP) from EGA-matched preterm infants without known neurological disease who required LPs for routine sepsis evaluation. Similarly, control CSF was acquired from full-term infants undergoing diagnostic LPs for a sepsis work-up. In all cases, the cultures for the CSF samples remained sterile. CSF samples from the operating room, NICU, or clinical laboratory were transported to the Washington University Neonatal CSF Repository on ice and then centrifuged at 2500 rpm for 6 min. The supernatant was then stored in microcentrifuge tubes at −80 °C until experimental analysis.

Automated Tandem, Multi-Affinity Fractionation of Human CSF—Multi-affinity fractionation (MAF) was performed on a BioCad Vision Work station, using a Cavro AFC 2000 autosampler/fraction collector. The affinity runs were monitored with an UV detector at 280 nm. The sample (2 ml) was applied to a IgY-14 affinity column (15 × 113 mm, Sigma-Aldrich). The components and fluid path configuration of the automated chromatograph is shown in supplemental Fig. S1. For automated MAF, an equal volume of 2 × TBS (20 mM Tris-HCl, 300 mM NaCl, pH = 7.4) was added to the frozen CSF samples (100 μl). After gentle inversion, the samples were filtered through a 0.45 μm filter unit (Millipore, Billerica MA). An 800 μl aliquot of the filtrate was taken and diluted to 2100 μl with 1 × TBS. The samples were run through an autosampler at 4 °C during MAF. Albumin, IgG, IgA, IgM, α_1-antitrypsin, transferrin, haptoglobin, apolipoprotein A1, apolipoprotein A2, fibrinogen, α_1-acid glycoprotein, α_2-macroglobulin, complement C3 and LD were removed with the first column (IgY-14) and the second in-line column (Supermix LC5 (12.7 × 39.5 mm), Sigma) removed the moderately abundant plasma proteins (14). The LC configuration (supplemental Fig. S1) also enabled the collection of bound proteins from both the columns by elution with 25 ml of 100 mM glycine Buffer, pH = 2.5 into fraction tubes containing 1 M triethyl ammonium bicarbonate, pH = 8.4. The affinity columns were neutralized with 100 mM Tris-Cl, pH = 8 and then re-equilibrated with TBS pH = 7.4. The flow-through and bound fractions were transferred to a centrifugal concentrating device (Amicon Ultra-15, nominal MCWO = 3 kDa) and spun to reduce the volume to ~300 μl.

Analytical One-Dimensional SDS-PAGE—The MAF was evaluated for reproducibility and molecular weight content in each fraction using analytical SDS-PAGE. Aliquots of fractions (10 μl) (15% of the total collected volume) were diluted with 5 μl of 4 × sample buffer (Bio-Rad Laboratories, Hercules, CA) and 1 μl 20 × reductant (Bio-Rad). The fractionated sample was heated to 95 °C for 5 min, cooled to room temperature and spun down at 13000 rpm for 30–60 s. The fraction samples were loaded on a 4–12% Criterion XT Bis-Tris gel

with molecular weight markers (Bio-Rad) and run in MES buffer. Once the blue dye front had run off the gel, the gel was removed and placed in fixative solution for at least 1 h. The gel was then stained with SyproRuby for at least 2 h, destained for 30 min and scanned on the Typhoon 9400 using the following settings: 457 nm excitation, 610BP30 emission filter, PMT voltage was adjusted to stay just below saturation for the darkest band.

Preparation of Peptides from MAF CSF—The concentrated, unbound eluates from the multi-affinity columns were precipitated using the vendor protocol for the two-dimensional clean-up kit (GE Healthcare, Pittsburgh, PA, Cat. No. 80–6484-51). The protein pellets were solubilized in 20 μl of Tris buffer (100 mM, pH 8.5) containing 8 M urea. The protein disulfide bonds were reduced with 1 mM tris(2-carboxyethyl) phosphine hydrochloride (2 μl of a 50 mM solution) (tris(2-carboxyethyl) phosphine hydrochloride bond breaker, 0.5 M solution, Thermo Fisher, Waltham, MA, Cat No. 77720) and placed at room temperature for 30 min. Alkylation of the cysteine residues was performed using iodoacetamide (2.2 μl of a 100 mM solution). After 30 min at room temperature in the dark, the reaction was quenched with 10 mM dithiothreitol at room temperature for 15 min. The reduced and alkylated proteins (~ 30 μl) were digested in 8 M urea with 1 μg of endoproteinase Lys-C (2 μl of a 0.5 μg/μl stock; Roche, Basel, Switzerland) after an overnight incubation at 37 °C. The samples were diluted 1:4 with 100 mM Tris, pH 8.5, trypsin (Sigma, Cat No. T6567) was added (~1:4 enzyme ratio), and the incubation was continued for 24 h at 37 °C. The digests were acidified with aqueous 5% formic acid (3.3 μl) (Fluka, St. Louis, MO, Cat No. 56302). The peptides were extracted with a conditioned Nutip carbon tip (Glygen, Columbia, MD, Cat No. NT3CAR). The tips were prepared by repetitive pipeting with 25 μl (x 3) of the peptide elution solvent (60% acetonitrile in 1% formic acid) and then equilibrated with 10 washes (25 μl) of extraction solvent (1% formic acid). The samples were loaded with 50 pipeting cycles. The tips were then washed four times with extraction solution. The peptides were recovered by 20 pipeting cycles with 25 μl of elution solution, followed by four washes (20 μl each) of elution solution. The extraction and wash solutions were combined in an autosampler vial (SunSri, Rockwood, TN, Cat No. 200 046) and dried in a SpeedVac (Thermo-Savant). The vial caps for the AS2 autosampler was from National Scientific (Rockwood, TN, Cat. No. 03-396AA).

High-resolution Nano-LC-MS—The complex mixtures of peptides from the endoprotease digests of the MAF samples were analyzed using high-resolution nano-LC-MS on hybrid mass spectrometers consisting of a linear quadrupole ion-trap and either a Fourier transform ion cyclotron (LTQ-FT) or an Orbitrap (LTQ-Orbitrap XL, Thermo Fisher Scientific). Chromatographic separations were performed using a nanoLC 1D Plus™ (Eksigent) for gradient delivery and a cHiPLC-nanoflex (Eksigent) equipped with a 15 cm × 75 μm C18 column (ChromXP C18-CL, 3 μm, 120 Å, Eksigent). The liquid chromatograph was interfaced to the mass spectrometers with a nanospray source (PicoView PV550; New Objective). Mobile phases were 1% formic acid (FA) in water (A) and 1% FA in 60% acetonitrile (B). After equilibrating the column in 98% solvent A (aqueous 1% FA) and 2% of solvent B (acetonitrile containing 1% FA), the samples (5 μl) were injected from autosampler vials using the LC-system's autosampler at a flow rate of 500 nL/min followed by gradient elution (250 nL/min) with solvent B: isocratic at 2% B, 0–5 min; 2% B to 25% B, 5–110 min; 25% to 80%, 110–170 min; 80% to 2%, 170–175; and isocratic at 2% B, 175–190 min. Total run time, including column equilibration, sample loading, and analysis was 217 min.

The maximum injection times for the MS1 scan in the Orbitrap and the LTQ were both 500 ms, and the maximum injection times for the MSn scan in the Orbitrap and the LTQ were 800 ms and 5000 ms, respectively. The automatic gain control targets for the Orbitrap and the LTQ were 5×10^5 and 3×10^4, respectively for the MS1 scans and 2×10^5 and 1×10^4, respectively for the MSn scans. The MS1 scans were followed by three MS2 events in the linear ion trap with collision activation in the ion trap (parent threshold = 10,000; isolation width = 4.0 Da; normalized collision energy = 30%; activation Q = 0.250; activation time = 30 ms). Dynamic exclusion was used to remove selected precursor ions (−0.20/+1.0 Da) for 90 s after MS2 acquisition. A repeat count of 3, a repeat duration of 45 s, and a maximum exclusion list size of 500 was used. The following ion source parameters were used: capillary temperature 200 °C, source voltage 2.5 kV, source current 100 μA, and the tube lens at 79 V. The data were acquired using Xcalibur, version 2.0.7 (Thermo Fisher). The operational parameters for LTQ-FT were as previously (15).

MS Data Processing and Protein Quantification—The LC-MS data processing pipeline is detailed in supplemental Fig. S12. For protein identification, the LC-MS/MS files that were acquired using Xcalibur were processed using Mascot Distiller software (version 2.0.3) for the preparation of files for database searching. A UniProt human protein database (downloaded December 2010, with 97,048 sequences) with an added BSA sequence (UniProt accession No., P02769) was searched using Mascot software (version 2.2.04) with the parameters given in the legend of supplemental Fig. S12. The protein database searches were further processed using Scaffold software (version 3_00_07) and the proteins were identified using the Protein Prophet algorithm (16) with protein and peptide thresholds of 95 and 50%, respectively. The identified peptide sequences and mass spectrometric data that were used for protein identifications are given in supplemental Table S1. The proteins were analyzed using knowledge-based network and pathway software, version 9 (Ingenuity® Systems, www.ingenuity.com).

For relative protein quantification, the LC-MS unprocessed files were imported into Rosetta Elucidator™ (Rosetta Biosoftware, ver 3.3) for retention time alignment of the peptide ion currents across the chromatographic time window using previously described parameters (17) and are detailed in supplemental Fig. S12. The aligned, normalized peptide ion currents were annotated after searching the UniProt database, as described above, within the alignment software by generating database search files (*.dta) and annotating at the feature level. The ion current signals from all charge states for each peptide were concatenated unique using a visual script within the software. The table of peptide sequences and peptide intensities was exported in Excel *.csv format. The peptides were grouped as individual genes (supplemental Tables S3 and S4). The gene-grouped and peptide intensity data were imported into DAnTE-R for statistical analysis (18, 19).

Knowledge-based Network Analysis—After false positive analysis (Protein Prophet) and removal of contaminants (*e.g.* keratins) and the set of IgY-14 and Supermix proteins, proteins as UNIPROT accession numbers were entered into the Ingenuity Pathways (www.ingenuity.com) (IPA, version 9.0, Redwood City, CA) as *.xls files. The software mapped all but four UniProt accession numbers, corresponding to gene symbols. Duplicate gene names that corresponded to the same gene were eliminated. A "core" analysis was performed using direct and indirect relationships, and limiting the Networks to 35 molecules per network. A total of 13 biological networks and pathways were generated from the input data ("focus genes") and gene objects in the Ingenuity Pathways (IPA) Knowledge Base. Networks with >3 gene objects are shown in Fig. 1 and supplemental Figs. S2–S11.

Confirmatory Analysis of Tandem MAF Proteomics in Serial CSF Samples—In order to confirm the protein changes observed with the tandem MAF proteomics technique, Western immunoblotting was performed using antibodies to beta-actin (ActB; Sigma, A-1978), apolipoprotein A-II (ApoA2; NovusBio, H00000336-MO3 (Littleton, CO)), amyloid precursor protein (APP; Covance Research Products (Princeton, NJ), neural cell adhesion molecule L1 (L1CAM; Thermo Scien-

tific, MA1–46044), LY6H lymphocyte antigen (Abcam, Cambridge, MA, ab55472), and the pigment epithelium-derived factor (SERPINF1; AbNova, MAB1077 (Taipei, Taiwan)), whereas an ELISA was performed for apolipoprotein A-IV (ApoA4; Millipore, EZHAPOA4–73K). For Western blots, 10 μl of CSF was mixed with 5 μl of sample buffer (Invitrogen, Carlsbad, CA; NP0007) and 2 μl of beta-mercaptoethanol. The solution was mixed, centrifuged, and heated at 70 °C for 10 min. Running buffer (1×) was made by combining MOPS running buffer 20X (Invitrogen; NP0001) and deionized water. Antioxidant (Invitrogen; NP0005) was added to make the cathode buffer. The samples were added into the wells of 4–12% Bis-Tris gels (Invitrogen; NP0336) and run for 70 min at 200 volts. Transfer buffer (1×) was made by mixing transfer buffer (20×; Invitrogen; NP00006) with deionized water, methanol, and antioxidant. The proteins were then transferred onto 0.45 μm pore size nitrocellulose membranes (Invitrogen, LC2006) for 150 min at 170 mA. The membranes were briefly washed in tris buffered saline - Tween 20 (TBST) and then blocked with 5% nonfat dry milk (Bio-Rad, Hercules, CA, 170–6404) for 1 h. The corresponding primary antibodies were then added at appropriate concentrations at 4 °C overnight. The following day the membranes were washed in TBST and the appropriate horseradish peroxidase (HRP)-linked secondary antibodies were added for one hour at room temperature. Chemiluminescence was then used to visualize the proteins of interest (Lumiglo; Cell Signaling Technology, Danvers, MA; 7003). The emitted light was read by the G:Box Chemi (Syngene, Frederick, MD) and digitized by the image acquisition software Genesnap (version 7.09.a; Synoptics; Cambridge, UK). Quantification of the band corresponding to the full-length protein was performed using ImageJ 1.45i (National Institutes of Health, USA), in which the integrated density (area × mean gray value) for the background of the membrane was subtracted from the integrated density of the full-length protein band. The mean and standard error for each group were then calculated and plotted, and used for statistical analysis.

For the ApoA4 ELISA, 20 μl CSF samples were incubated in wells precoated with polyclonal anti-human ApoA4 antibody for 2 h at room temperature. The wells were washed, and 100 μl of secondary biotinylated polyclonal anti-human ApoA4 antibody was added for 1 h at room temperature. After washing, 100 μl streptavidin-HRP conjugate solution was added for 30 min. After a final washing, 100 μl of 3,3′,5,5′-tetramethylbenzidine was added for 20 min, followed by 100 μl of stop solution. The ApoA4 ELISA was run in triplicate, and the 96-well plates were read at 450 nm in a Versamax microplate reader (Molecular Devices, Sunnyvale, CA). Actual concentrations were determined using a four parameter logistic standard curve as detailed by the manufacturer.

For these confirmatory studies (both Westerns and ELISAs), two CSF samples (S1, S2) were obtained from a single subject separated in time by 1 week. For each protein analyzed, samples were run in triplicate and compared as detailed in "Statistical Analyses" below. In order to assess the effect of tandem MAF on the abundance of specific proteins and trends in their respective levels with PHH treatment, we used Westerns and ELISAs to analyze the levels of ActB and ApoA4 before and after tandem MAF. APP, L1CAM, ApoA2, SERPINF1, and LY6H levels also were examined by Western blot in S1 and S2.

Conventional Methods Utilized to Evaluate the Effect of PHH Treatment on Protein Mediators of Neurodevelopment—Both ELISAs and Western blots were used to examine CSF levels of several protein mediators of neurodevelopment throughout the PHH treatment interval and in-age-matched control CSF samples. L1CAM levels were measured using a commercially available ELISA kit (DRG, catalog #EIA5074, Mountainside, NJ). Similar to the ELISA described above for ApoA4, pre-coated plates were filled with 50 μl of CSF, followed by the enzyme conjugate provided for 1 h. Plates were washed, and 100 μl of enzyme complex was added for 30 min. After final washings, 100 μl of substrate solution was incubated for 15 min, followed by the addition of 100 μl of stop solution.

DuoSet ELISA development systems (R&D Systems, catalogue # DY-850 and DY-2408, Minneapolis, MN) were used to measure APP and the neural cell adhesion molecule 1 (NCAM-1). High-binding polystyrene microplates (Costar, Corning Life Sciences, Inc., Lowell, MA) were coated overnight at room temperature with 2 μg/ml of mouse monoclonal anti-human APP or NCAM-1 primary antibody diluted in phosphate-buffered saline (PBS). The plate was washed with 0.05% Tween 20 in PBS and blocked using 1% bovine serum albumin (BSA) in PBS. CSF samples were diluted 1:100 in 1% BSA in PBS, and 100 μl were incubated for 2 h at room temperature. After washes, 100 μl of 200 ng/ml biotinylated goat anti-human APP or NCAM-1 secondary antibody was added and incubated for 2 h at room temperature. The samples were washed once again and 100 μl of streptavidin-HRP, diluted 1:200 in 1% BSA in PBS was added for 20 min at room temperature. After the final wash, 100 μl of equal volumes stabilized hydrogen peroxide and stabilized tetramethylbenzidine was loaded and incubated for 20 min at room temperature. Lastly, 50 μl 2N sulfuric acid was added to stop the reaction.

As described above, the APP, L1CAM, and NCAM-1 ELISAs were run in duplicate, and the 96-well plates were read at 450 nm on a Versamax microplate reader (Molecular Devices, Sunnyvale, CA). Actual concentrations were determined using a four parameter logistic standard curve as detailed by the manufacturers.

Western blots were run in triplicate and analysis was performed as described above to detect differences in full-length brevican (BCAN; R&D Systems, MAB4009), calsyntenin 1 (CLSTN1; Lifespan Biosciences, C110964), matrix metalloproteinase-9 (MMP9; Novus Bio, NB100–2290), and neurocan core protein (NCAN; Novus Bio, NBP1–07069).

ELISA analyses for APP, NCAM-1, and L1CAM utilized an average of 12 PHH and 24 control CSF samples obtained from infants of various gestational ages. Western analyses compared 12 PHH with 12 control CSF samples.

Statistical Analyses—For the confirmatory studies evaluating the effect of tandem MAF in serial samples, (Western blots and ApoA4 ELISA), differences between S1 and S2 values were compared with Student's *t* test or an ANOVA with a Tukey post hoc test, as appropriate (GraphPad Prism Statistics 5.03, La Jolla, CA). Results are expressed as means ± S.E. (S.E.). Significance was defined as p value <0.05. This method of statistical analysis was also used for the Western blots presented in supplemental Figs. S13 and S14.

For the longitudinal studies of L1CAM, APP, NCAM, and BCAN, PHH and control regression lines were fit simultaneously with a weighted least squares multiple regression (PROC REG, SAS 9.2 Cary NC) in which the weight was the inverse variance estimate from the corresponding simple regressions. Separation of 95% confidence intervals was used to identify predicted means that differ.

RESULTS

Knowledge-based Analysis of Proteins Identified in CSF From Preterm Infants with PHH—Our first goal was to determine if a multi-affinity approach developed for abundant proteins in plasma (14) would enable us to reliably identify and quantify brain proteins in blood-containing CSF. We used two types of MAF columns, IgY-14 and Supermix, assembled in series to remove high- and moderate-abundance plasma proteins, respectively, from CSF. After sequential MAF of CSF (0.5 ml) (supplemental Fig. S1), we analyzed the peptides from the unretained proteins using LC-MS. We identified 438 pro-

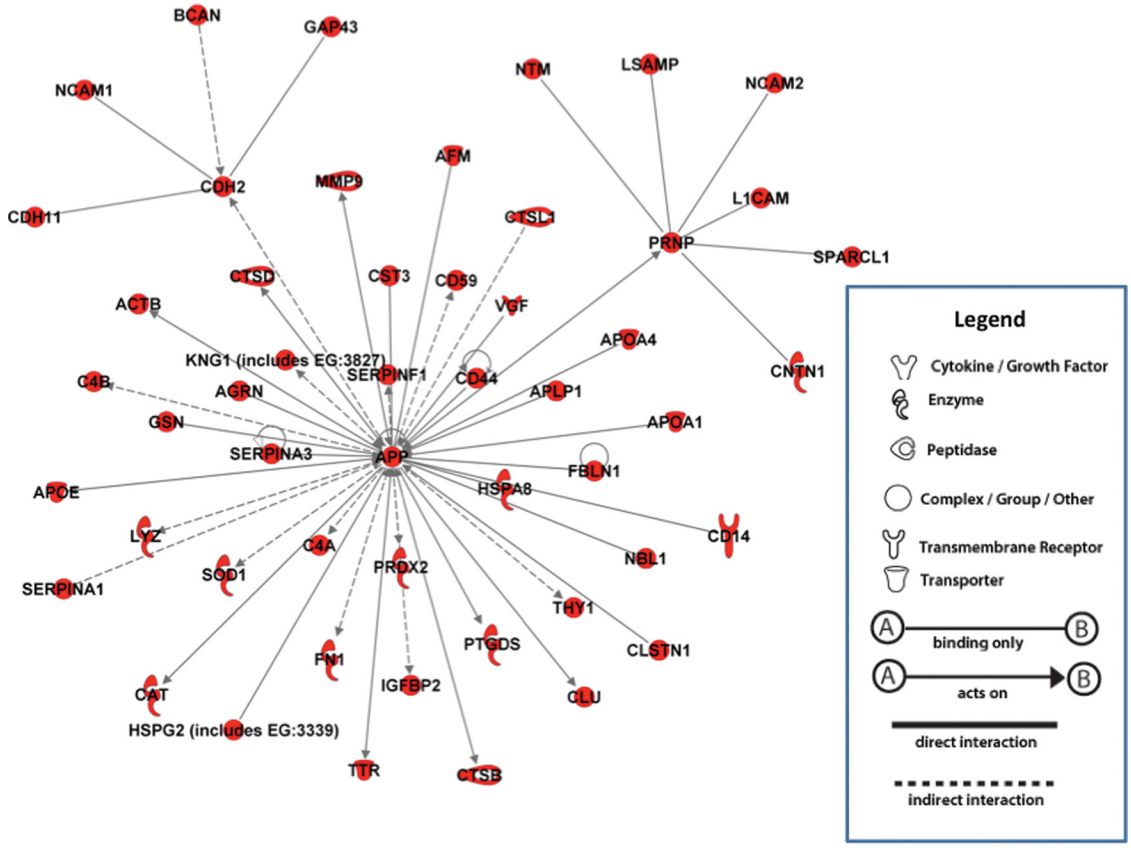

FIG. 1. **Pathway analysis of neurodevelopmental proteins identified in CSF of posthemorrhagic hydrocephalus.** Network 1 resulting from the Ingenuity Pathways Analysis comprising the proteins identified in PHH CSF, including APP, L1CAM, BCAN, and NCAM-1. Additional networks that were mapped to gene objects in the IPA database are shown in supplemental Figs. S2–S11. As shown in the legend, nodes represent genes, with specific shapes denoting protein functional classes. Direct and indirect relationships between nodes are shown as unbroken or dashed lines indicating, respectively.

teins after searching the human protein database, using Protein Prophet algorithm (supplemental Table S1). After removal of hemoglobin, plasma proteins that are efficiently removed by the two MAF columns (14), and contaminant proteins (*e.g.* keratin), we uploaded the proteins into Ingenuity Pathway software (IPA) for knowledge-based software analysis. The proteins were mapped to 11 biological networks (supplemental Table S2; networks with >3 gene objects are shown in supplemental Figs. S2–S11).

Fig. 1 shows IPA Network 1, which consists of proteins with well-characterized roles in nervous system development. Each gene object pictured corresponds to a protein observed in PHH CSF. Broadly, the PHH CSF proteins within this network may be classified according to their localization or role in neurodevelopment (Table I). L1CAM, NCAM-1, neurotrimmin, and contactin 1 function as cell adhesion molecules. Of this group, L1CAM and NCAM-1 are of particular interest because of their role in axonal guidance and cell migration. Further, L1CAM has well-characterized involvement in congenital hydrocephalus and severe neurological disability (20, 21). Among the membrane-associated proteins noted in the PHH CSF were APP and CLSTN1. APP is believed to be involved in neurite outgrowth, synaptogenesis, and cell migration but also is known for its role in the cognitive dysfunction observed in Alzheimer's disease (22). CLSTN1 is known to stabilize APP metabolism and accumulate in dystrophic neurites around the amyloid core of Alzheimer's disease senile plaques (23, 24). Several proteins in the PHH CSF samples were either components of the extracellular matrix (ECM) itself or were involved in the regulation or maintenance of the ECM (*e.g.* MMP9). The proteoglycan BCAN is an important ECM component that has been shown to stabilize synapses, promote neurite outgrowth, and facilitate myelination. Excessive deposition of BCAN has been implicated in the disruption of cellular architecture and glial scarring observed following neonatal hypoxia-ischemia (25) and could have a similar effect in PHH. MMP9 is involved in the regulation of ECM and thus modifies multiple neurodevelopmental processes, including cell attachment, proliferation, differentiation, migration, and apoptosis (26). The cytoskeletal proteins beta actin and the actin-binding protein gelsolin also were observed in PHH CSF. Beta-actin participates in many important neurodevelopmental processes, including synaptogenesis, collateral branching, and neuronal migration (27–30). Gelsolin normally

TABLE I

Classification of protein mediators of neurodevelopment observed in CSF from post-hemorrhagic hydrocephalus. Also, shown in Fig. 1, these proteins observed in PHH CSF were mapped to network 1 by IPA

Cell Adhesion Regulators			*Extracellular Matrix Regulators*	
CD44	L1CAM		AGRN	Hspg
CDH2	LSAMP		BCAN	HSPG2
CDH11	NCAM1		COL18A1	MMP9
CLU	NCAM2		FBLN1	SPARCL1
CNTN1	NTM			
Membrane-Associated			*Intracellular Enzymes*	
APLP1	GAP43		CTSB	HSPA8
APP	PRNP		CTSD	PTGDS
CD14	CD59		CTSL1	SOD1
CLSTN1	THY1		Hsp70	
Cytoskeleton Regulators			*Protease Inhibitors*	
ACTB	GSN		CST3	SERPINA3
Extracellular Enzymes			*Anti-oxidants*	
CAT	TTR		APOA4	PRDX2
NBL1			APOE	
Growth Factors and Neurotrophic Proteins				
IGFBP2	SERPINF1	VGF		

is involved in actin assembly and regulation through capping and severing (31). Both beta actin and gelsolin have been implicated in various neurological diseases, such as multiple sclerosis, Alzheimer's and HIV-related dementia, and dystonia (32–34). Another protein of interest was the neurotrophin SERPINF1, which has been shown to induce neuronal differentiation in various cell types, including retinoblastoma lines (35, 36). A number of growth regulators (neurosecretory protein VGF, insulin-like growth factor binding protein), enzymes, protease inhibitors, and anti-oxidants were also observed in the PHH CSF (Table I).

Quantification of Proteins After Treatment Using Label-free Quantitative Proteomics—The confident identification of biological changes in protein abundances using label-free proteomics methods requires the measurement of technical variability in individual proteins. We determined the technical reproducibility of our proteomic workflow, including MAF, preparation of peptides, and nano-LC-MS. Fig. 2*A* shows the replicate experimental design for CSF samples that were procured 1 week apart from an individual PHH infant. To minimize the variability that is associated with MAF (14), we used an automated liquid chromatograph for the removal of high and medium abundance plasma proteins (supplemental Fig. S1). The MAF sample preparation of the eight peptide preparations were randomized to minimize bias associated with column batch effects (37). The 1D PAGE analysis of the nonretained proteins from the eight MAF runs is shown in Fig. 2*B*, with only minor differences in band intensities apparent among the samples. Peptide pools were prepared from the concentrated, unbound proteins by sequential endoprotease digestion and the complex peptide mixtures were analyzed in random order using high-resolution LC-MS. The data processing and analysis pipeline is detailed under "Experimental Procedures" and in supplemental Fig. S12. Briefly, the data-dependent nano-LC-MS individual runs were processed using Rosetta Elucidator™ software to identify 69,717 features that were intensity scaled to the mean of all the integrated peptide intensities (17) for individual LC-MS runs. The peptide ion chromatograms from the LC-MS analyses were aligned using retention time and high-resolution *m/z* measurements. After intensity normalization, technical replicate reproducibility was first assessed by comparing the distribution of coefficients of variation (CV) of the isotope group intensities from each biological sample (Fig. 2*B*). A similar distribution was observed with the percentage of isotope groups (S1 = 17,190; S2 = 17,513) with intensity CVs of $< 50\%$ (81.1% and 90.2% for CSF procurements S1 and S2, respectively). These results are similar to that previously reported for label-free quantitative proteomics measurements (33, 38, 39). As a measure of peptide preparation reproducibility, equivalent amounts of an internal standard protein, BSA was added to each sample prior to endoprotease digestion. Fig. 2*C* shows the intensities of a BSA peptide that has a unique sequence compared with all tryptic peptides from human albumin, LFTFHADICTLPDTEK. The CV of this peptide was 27.5%, and the CV of all observed "bovine unique" peptides was 32%. In Fig. 2*D*, the intensities of an L1CAM peptide are shown for the two procurements, demonstrating, from these normalized peptide intensity measurements of a single peptide, a consistent decrement in the S2 samples. To identify the peptide signals that showed a statistically significant difference between the two procurements, the summed signals from individual peptides (isotope groups) were statistically analyzed by ANOVA followed by unsupervised hierarchical clustering. The peptide signals (*e.g.* isotope groups) with a charge state of greater than +1 (15, 993) were analyzed for statistically significant differences ($p < 0.001$) between the two procurements, each with quadruplicate MAF replicates. These "differential" peptide intensities (3433) were then analyzed by hierarchical cluster analysis as shown in Fig. 2*E*. The two biological samples were clearly distinguished by the clustering algorithm with 1739 and 1691 peptide intensities increased in samples S1

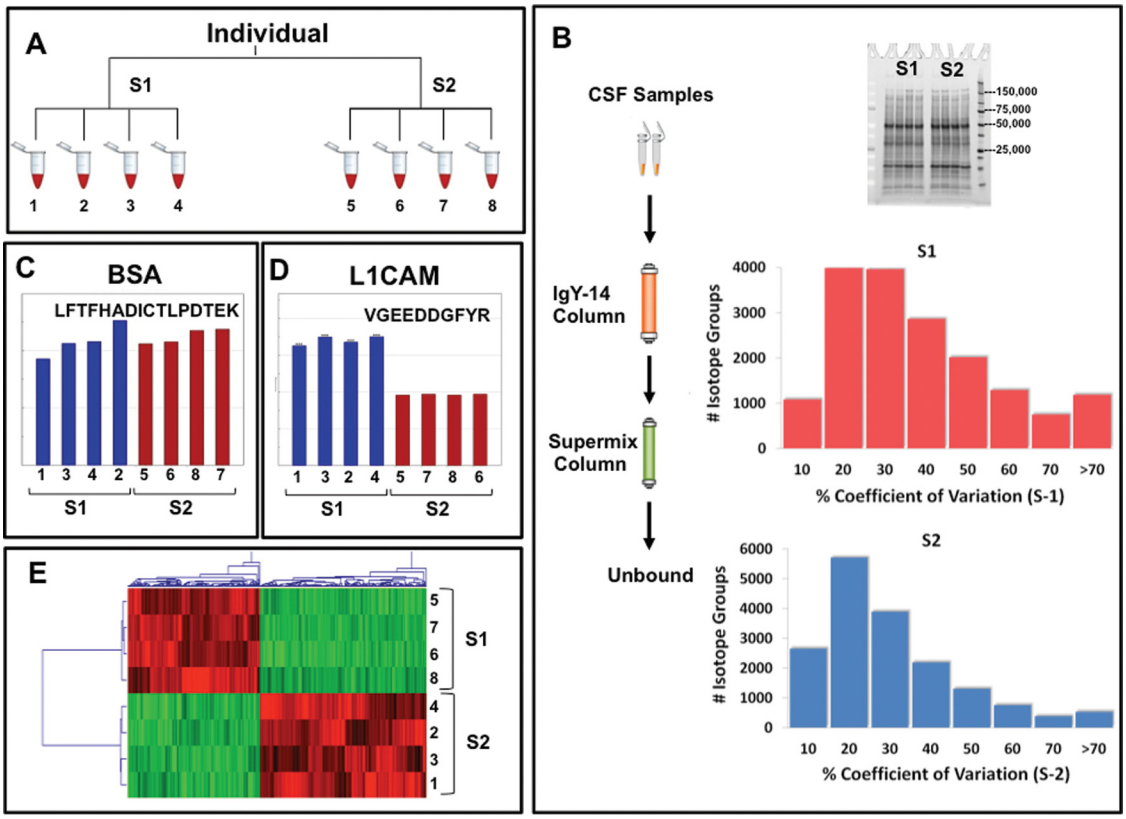

FIG. 2. **Tandem multi-affinity fractionation yields consistent samples for LC-MS analysis with limited technical variability.** *A*, Experimental design for label-free protein quantification of two CSF procurements S1 and S2 obtained 7 days apart from a single infant after initiation of treatment for PHH. Four multi-affinity fractionations were performed for each sample and analyzed in a randomized fashion as follows: S1.2, S1.1, S1.4, S2.3, S2.2, S2.1, S2.4, and S1.3. *B*, SDS-PAGE analysis of the four MAF replicates from S1 and S2. The distributions of the coefficient of variation for the peptide ion intensities from LC-MS analysis is plotted for the observed peptide signals as isotope groups. *C*, Peptide ion intensities for bovine serum albumin from the indicated internal standard peptide from S1 (blue bars) and S2 (red bars, and the individual samples as designated in *A*. *D*, Peptide ion intensities of the indicated L1CAM peptide from S1 (blue bars) and S2 (red bars, and the individual samples as designated in *A*). *E*, Hierarchical cluster analysis of significant peptide intensities ($p > 0.001$) after ANOVA statistical analysis as described under "Experimental Procedures." The LC-MS analysis order was as follows: S1.3, S2.3, S2.2, S1.4, S1.1, S1.2, S2.4, and S2.1.

and S2, respectively. Among the proteins with differential peptides in the peptide intensity heat map was L1CAM. Fig. 3*A* shows the relative intensities of the six peptides that were identified for L1CAM. Peptide intensities have been converted to a Z score statistic for comparison on a scale of standard deviation values that are centered on a mean of zero. The intensities from the individual peptides are ordered across the eight samples. Most of the peptide values in the earlier PHH sample (S1) are higher than in the sample obtained 1 week later (S2). As has been well-described for label-free quantitative proteomics analysis of complex samples, peptide intensities for an individual protein can demonstrate considerable variability, which can be assessed with "rollup" methods that account for this variability when calculating fold changes and *p* values for protein abundance changes (19). Using the DAnTE open-source proteomics software program (http://omics.pnl.gov/software/), we determined the fold change between these two samples spaced closely in time for L1CAM to be 2.07 with a *p* value <0.0001. In Fig. 3*B*, the three peptides that were identified for APP showed a uniform trend in the standardized intensities with a fold change of 6.22 and a *p* value <0.0001 for the change in protein abundance. Chromagranin A (CHGA; Fig. 3*C*) is shown as an example of a protein in which the standardized peptide intensities demonstrate significantly greater dispersion, both at the individual peptide level and for different samples. Fractions 3 and 7 show consistent trends for the eight peptides (decreased in the S2 samples); however, no obvious trend is seen in the other preparations. We speculated that some proteins may be difficult to quantify because of idiosyncratic peptide production in the endoprotease digestions or loss of peptides from endogenous proteolytic digestions during preparation. This data dispersion is reflected in the much higher *p* value for CHGA. To examine the trends in the protein level data, unsupervised hierarchical clustering was performed of the protein level values after rollup. In the heat map (Fig. 3*D*), the high variability of CHGA can be observed, in which an intensity bar is evident in fraction 3 and a black bar in

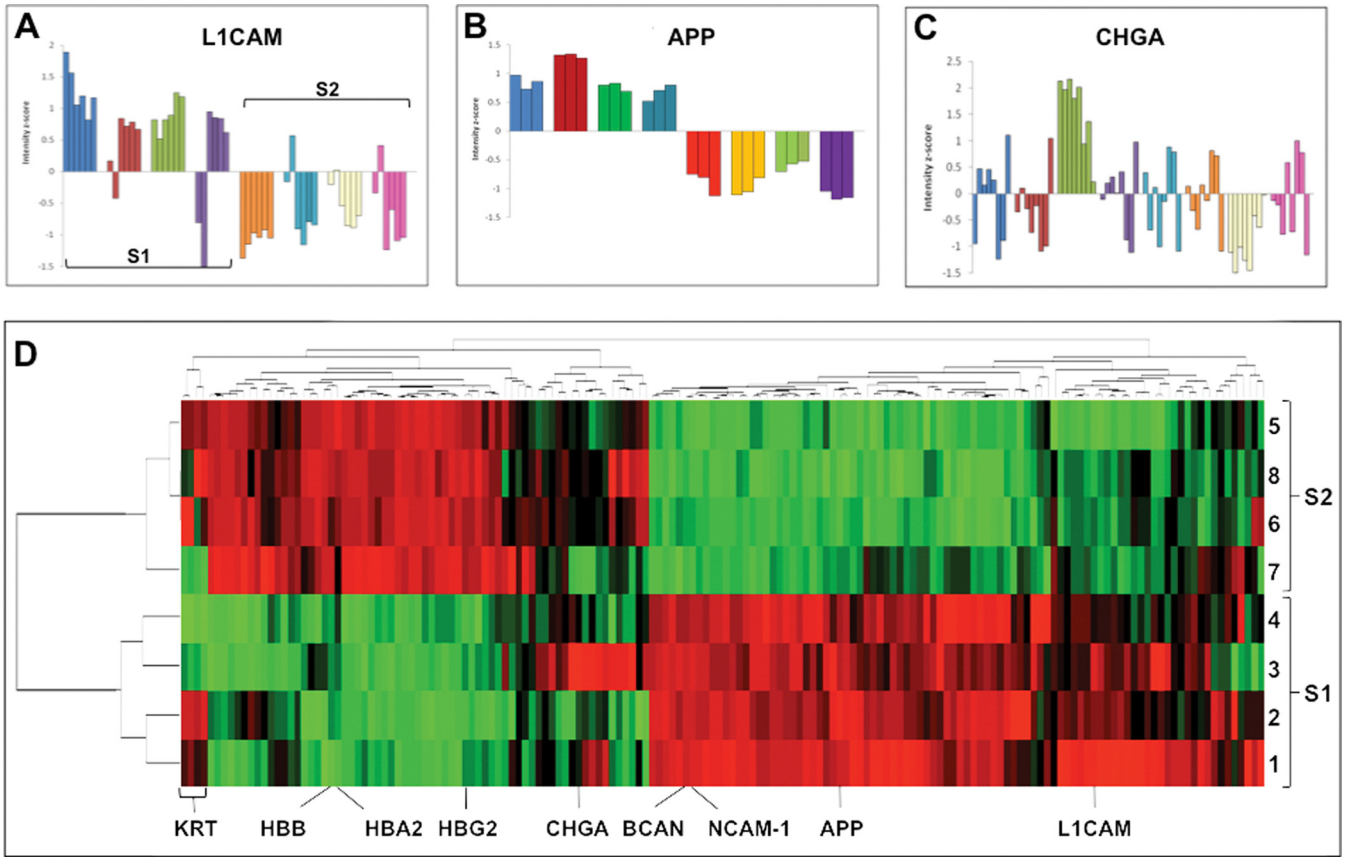

FIG. 3. **Tandem MAF-quantitative proteomics demonstrates consistent changes at the peptide and protein level in the CSF of preterm infants during treatment for PHH.** Replicate fractions from two CSF procurements (S1 and S2) obtained 7 days apart from a single infant after initiation of treatment for PHH. Shown are the standardized peptide intensities of the 6 L1CAM peptides (*A*), the 3 APP peptides (*B*), and the eight chromagranin A peptides (*C*). Bar coloring is used to differentiate standardized peptide intensities by replicate fraction for both S1 and S2.Standardized intensities were calculated as described under "Experimental Procedures." The peptides and their normalized intensity values are given in supplemental Table S3. *D*, Hierarchical cluster analysis of the mean intensity z score for all proteins that were identified with two or more peptides, both with a Mascot score of > 40. Several proteins of interest are highlighted (KRT: Keratin; HBB: Hemoglobin beta; HBA2: Hemoglobin alpha 2; HBG2: Hemoglobin gamma G; CHGA: Chromogranin A; BCAN: Brevican; NCAM1: Neural cell adhesion molecule 1; APP: Amyloid precursor protein; L1CAM: L1 cell adhesion molecule).

fraction 8. Other proteins that were significantly different ($p < 0.05$) in abundance between the two procurements, including L1CAM and APP, showed more consistent patterns. Keratins that are well recognized as random contaminants in proteomics analyses showed increased levels in samples 1, 2, 6, and 5.

Confirmatory Analysis of Tandem MAF-Proteomics Using Conventional Experimental Techniques—Based on the results of the tandem MAF proteomic analysis, ApoA4 ELISAs were performed for PHH CSF samples S1 and S2, and Western blots were performed for beta actin, APP, L1CAM, LY6H, and SERPINF1. Fig. 4*A*, shows a comparison of ApoA4 concentrations in naive PHH CSF samples (before tandem MAF) to those in immunodepleted (ID) samples (after tandem MAF); it is clear that tandem MAF efficiently removed ApoA4 in both S1 and S2. Notably, the increase in ApoA4 levels observed in S2 relative to S1 in naive samples (19283 $\pm$ 57.5 ng/ml *versus* 7478.54 $\pm$ 23.01 ng/ml, $p < 0.0001$) was replicated, albeit with dramatically lower levels, in the ID samples (0 ng/ml *versus* 210.217 $\pm$ 19.11 ng/ml, $p < 0.05$). ActB (Fig. 4*B*) showed similar results, with an overall decrease in levels in both S1 and S2 following tandem MAF. An increase in levels between naive S1 (391820 $\pm$ 20571) and naive S2 (695328 $\pm$ 22787) was noted ($p = 0.0006$), though after tandem MAF this difference was no longer significant ($p = 0.204$).

Fig. 5*A*, shows a scatter plot summarizing the quantitative ANOVA data for proteins from Network 1 that demonstrate significant differences between S1 and S2. This volcano plot, in which p values from the ANOVA analysis of rollup peptide intensities are plotted against $\log_2$ fold-change, shows that 16 proteins were decreased in S2 (after 7 days of PHH treatment), whereas 10 were increased, and 20 were unchanged. The fold-change values between S1 and S2 and their corresponding p values are summarized in Table II.

Additional confirmatory studies were performed with Western blots for APP and L1CAM (Fig. 5*B*). The decreasing levels

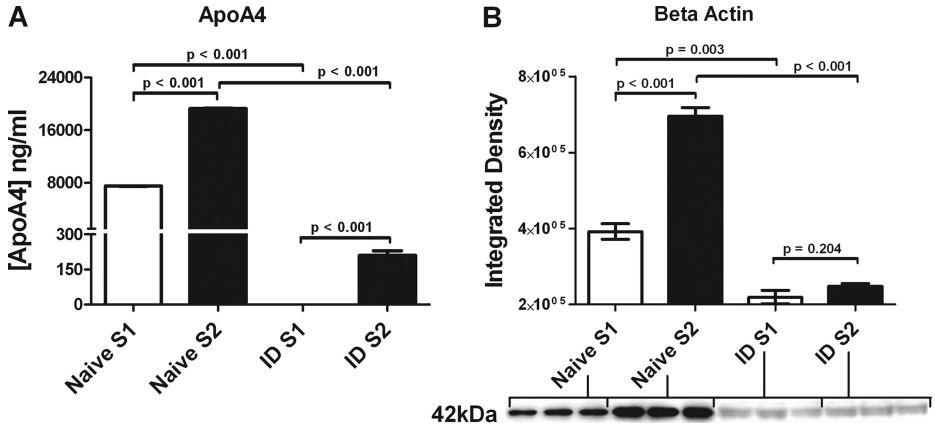

FIG. 4. **Confirmation of immunodepletion in tandem multi-affinity fractionation.** *A*, The concentration of ApoA4 shown in naive (before tandem MAF) and immunodepleted (ID, after tandem MAF) S1 and S2 CSF samples. *B*, The relative levels of the full length isoform of beta-actin (ActB) in naive and ID S1 and S2 CSF. Note that after tandem MAF, the levels of ApoA4 and beta-actin were dramatically and significantly reduced.

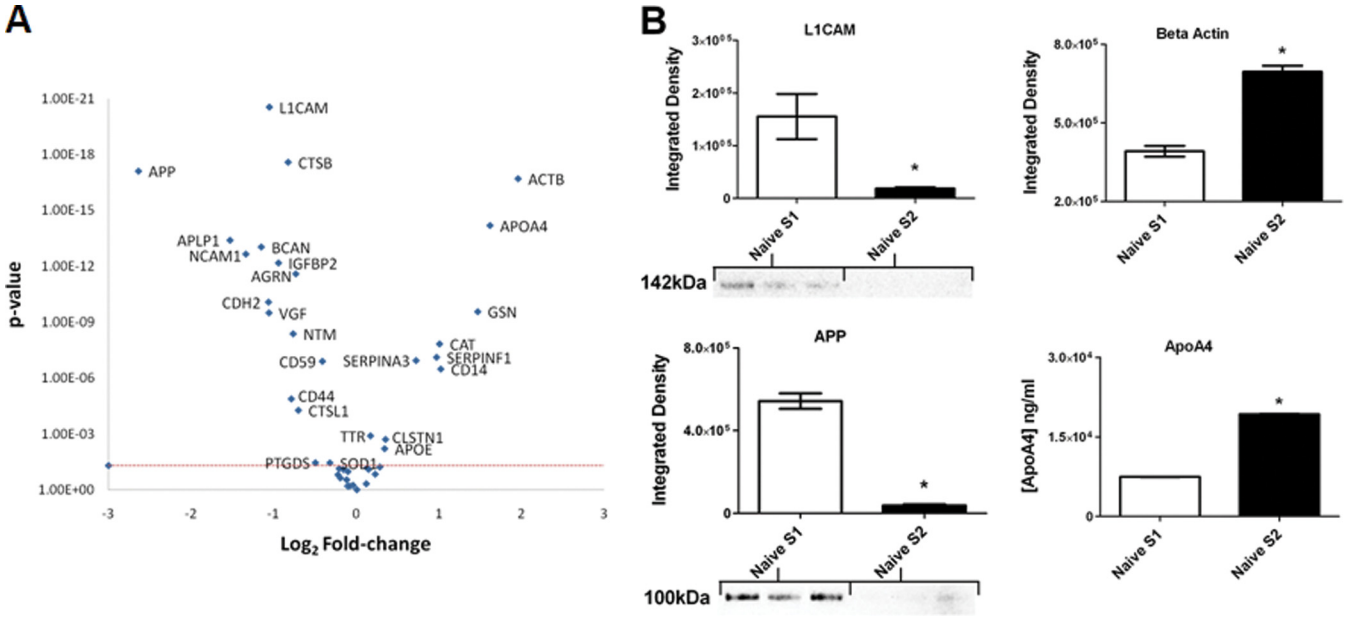

FIG. 5. **Changes in the CSF levels of protein mediators of neurodevelopment after initiation PHH treatment are protein-specific.** *A*, Volcano plot showing changes in the relative abundances of CSF protein mediators of neurodevelopment identified with tandem MAF proteomics after initiation of PHH treatment. The *p* values from the Benjamini-Hochberg-corrected ANOVA results are plotted against the $\log_2$ fold change. The proteins shown are the quantifiable proteins from the neurodevelopmental pathway shown in Fig. 1. After initiation of PHH treatment, proteins displayed a decrease (left of 0 on the axis), increase (right of 0), or no significant change at all (below the hashed red line). Note the decrease in APP and L1CAM over the 7 day interval from S1 to S2, whereas ActB and ApoA4 increase. Fold-change measurements for the proteins demonstrating a significant difference between samples are shown in Table II. *B*, Conventional laboratory techniques including Western blot (L1CAM, APP, and ActB) and ELISA (ApoA4) confirm the trends in protein levels observed with tandem MAF process. The immunoblot for beta actin was shown in the previous figure. Asterisks denote $p < 0.05$, $n = 3$ per group.

of L1CAM and APP observed with Western blots closely mimicked the results seen with tandem MAF-proteomics (L1CAM was 155364 ± 43107 in S1 *versus* 18437 ± 2585 in S2, $p = 0.03$; APP was 542826 ± 37205 in S1 *versus* 38022 ± 6395 in S2, $p = 0.0002$). Results of the ApoA4 ELISA and ActB Western blot, both examples of proteins that increase in S2, are shown in Fig. 5*B* for reference. Although a statistical significance was not observed in a confirmatory Western blot for SERPINF1, the increasing trend observed with tandem MAF-proteomics was reproduced with Western blotting ($p = 0.12$; data not shown). Investigating proteins outside of the network, ApoA2 and LY6H were examined for consistency with the tandem MAF-proteomics results (supplemental Fig. S13); both showed agreement with the proteomics findings, though the *p* value for LY6H did not reach significance ($p = 0.2$).

TABLE II

Protein mediators of neurodevelopment showing significant alterations in CSF levels between samples obtained at the initiation of clinical PHH treatment (S1) and one week later (S2). Each protein was mapped to network 1 using IPA

Index No.	Gene Symbol	Protein Description	Fold-change	*p* value
Decreased				
29	APP	Amyloid beta A4 protein	6.22	8.02E-18
20	APLP1	Amyloid-like protein 1	2.88	4.12E-14
279	NCAM1	Neural cell adhesion molecule 1	2.52	2.28E-13
40	BCAN	Brevican core protein	2.22	9.47E-14
79	CDH2	Cadherin-2	2.09	8.68E-11
420	VGF	Neurosecretory protein VGF	2.08	3.27E-10
241	L1CAM	Neural cell adhesion molecule L1	2.07	2.91E-21
213	IGFBP2	Insulin-like growth factor-binding protein 2	1.92	6.85E-13
123	CTSB	Cathepsin B	1.77	2.66E-18
73	CD44	CD44 antigen	1.72	1.31E-05
298	NTM	Neurotrimin	1.7	4.20E-09
9	AGRN	Agrin	1.66	2.63E-12
126	CTSL1	Cathepsin L1	1.62	5.37E-05
334	PTGDS	Prostaglandin-H2 D-isomerase	1.41	3.54E-02
74	CD59	CD59 glycoprotein	1.33	1.26E-07
383	SOD1	Superoxide dismutase [Cu-Zn]	1.25	3.58E-02
Increased				
3	ACTB	Actin, cytoplasmic 1	3.9	2.04E-17
24	APOA4	Apolipoprotein A-IV	3.08	6.64E-15
184	GSN	Gelsolin	2.78	2.83E-10
70	CD14	Monocyte differentiation antigen CD14	2.04	3.27E-07
68	CAT	Catalase	2.01	1.47E-08
369	SERPINF1	Pigment epithelium-derived factor	1.97	7.63E-08
364	SERPINA3	Alpha-1-antichymotrypsin	1.65	1.14E-07
95	CLSTN1	Calsyntenin-1	1.28	1.97E-03
27	APOE	Apolipoprotein E	1.27	6.16E-03
415	TTR	Transthyretin	1.13	1.27E-03

Comparative Tandem MAF LC-MS Proteomics Demonstrated a Unique CSF Peptide Signature in PHH—Utilizing this novel application of tandem MAF LC-MS proteomics, a comparative study was conducted to test for differences in CSF proteins in PHH *versus* age-matched control preterm infants. In PHH infants, CSF was obtained upon cannulation of the ventricle (initial sample, or IS) during placement of a ventricular reservoir to initiate clinical treatment of PHH. CSF was also obtained in these same infants at TEA when they underwent implantation of a permanent VP shunt. In sum, a total of 69,717 (25,148 charge groups) *m/z* features were detected and time aligned.

Overall, the levels of 159 proteins were found to be significantly altered in PHH_{IS} *versus* control CSF, with the majority showing elevations in PHH. Table III provides a listing of the Network 1 CSF proteins that showed differences in PHH_{IS} and control (for a complete list see supplemental Table S5). Among these proteins were several key regulators of neurodevelopment, including L1CAM, APP, BCAN, and NCAM-1. These proteins were chosen for further study based on their magnitude of fold-change in PHH over control and their well-characterized roles in neurodevelopment and/or neurological disability. On the tandem MAF-proteomics analysis, L1CAM, APP, and BCAN exhibited 4.96-, 10.4-, and 8.17-fold increases, respectively, when PHH_{IS} was compared with age-matched controls ($p < 0.01$ for all, Fig. 6*A*–6*C* insets). After 8 weeks of treatment (PHH_{TEA}), the observed elevations in L1CAM, APP, and BCAN resolved, and levels were no longer different than control. NCAM-1 showed a similar increase in PHH_{IS} (2.55 fold increase over control) but differed from the other proteins in its incomplete resolution at PHH_{TEA} (NCAM-1 PHH_{TEA} *versus* control $p = 0.02$; PHH_{TEA} *versus* PHH_{IS} $p < 0.001$; Fig. 6*D* inset).

Fig. 6*A*–6*D*, show the protein levels of L1CAM, APP, BCAN, and NCAM-1 in CSF of preterm infants undergoing treatment for PHH compared with a cohort of EGA-matched controls. L1CAM, APP, and NCAM-1 were quantified with ELISAs, whereas a Western blot was used to assess BCAN. Each protein demonstrated increased levels at PHH_{IS}, but these elevations resolved with time as clinical treatment was undertaken. However, the rate of decrease, and thus the time to resolution of each protein elevation (approximated by the slope of the fit line), varied by protein. As described in the "Experimental Procedures" section, these outcomes were fit with a least squares multiple regression and a separation of 95% confidence intervals were used to identify predicted means that differ. With treatment, the initially increased levels of L1CAM and APP (Figs. 6*A* and 6*B*) had lost their significance between PHH and control CSF by 36

TABLE III

Protein mediators of neurodevelopment exhibiting significant differences between initial PHH samples (PHH_{IS}) and age-matched preterm infants with no known neurological injury or disease (control). Each protein was mapped to the network 1 using IPA

Index No.	Gene Symbol	Protein Description	Fold-change	*p* value
Decreased				
325	PRDX2	Peroxiredoxin-2	1050	4.67E-40
68	CAT	Catalase	501	1.56E-48
123	CTSB	Cathepsin B	78.8	1.04E-25
273	MMP9	Matrix metalloproteinase-9	45.8	2.22E-18
3	ACTB	Actin, cytoplasmic 1	34	8.36E-15
70	CD14	Monocyte differentiation antigen	29.3	4.00E-22
96	CLU	Clusterin	24	8.04E-23
415	TTR	Transthyretin	19.8	5.64E-14
280	NCAM2	Neural cell adhesion molecule 2	17.9	1.40E-07
95	CLSTN1	Calsyntenin-1	12.3	1.99E-26
29	APP	Amyloid beta A4 protein	10.4	2.22E-27
383	SOD1	Superoxide dismutase [Cu-Zn]	9.41	3.28E-11
40	BCAN	Brevican core protein	8.17	3.63E-12
79	CDH2	Cadherin-2	6.31	6.40E-15
213	IGFBP2	Insulin-like growth factor-binding protein 2	6.08	2.71E-20
27	APOE	Apolipoprotein E	6.05	3.57E-04
24	APOA4	Apolipoprotein A-IV	5.78	3.58E-12
184	GSN	Gelsolin	4.97	2.60E-11
241	L1CAM	Neural cell adhesion molecule L1	4.96	1.56E-19
171	GAP43	Neuromodulin	3.21	5.17E-04
209	HSPG2	Basement membrane-specific heparan sulfate proteoglycan core protein	3.09	1.81E-09
9	AGRN	Agrin	2.93	2.31E-12
20	APLP1	Amyloid-like protein 1	2.82	1.10E-08
279	NCAM1	Neural cell adhesion molecule 1	2.55	4.81E-09
99	CNTN1	Contactin-1	2.42	1.02E-03
155	FBLN1	Fibulin 1	2.18	2.81E-04
369	SERPINF1	Pigment epithelium-derived factor	2.15	4.49E-07
388	SPARCL1	Proliferation-inducing protein 33	1.76	7.62E-03
118	CST3	Cystatin-C	1.5	4.16E-02
Increased				
278	NBL1	Neuroblastoma, suppression of tumorigenicity 1	8.17	9.23E-09

weeks (34.5 for L1CAM and 35.5 for APP). A similar, albeit at a slower rate, trend was observed in BCAN and NCAM-1 (Figs. 6*C* and 6*D*). These two proteins remained statistically significantly different until TEA; 37 weeks and 40 weeks, respectively.

Supplemental Fig. S14 shows the Western analysis for proteins CLSTN1 (panel A) and MMP9 (panel B). Referring to Table III, both proteins showed an impressive increase in PHH_{IS} over age-matched controls (12.3 and 45.8 fold-increase, respectively). The Western analysis confirmed these findings; both proteins showed significant increases in PHH_{IS} levels over age-matched controls (CLSTN1, $p = 0.03$; MMP9, $p = 0.008$), and the levels returned to control levels at TEA (CLSTN1, $p = 0.88$; MMP9, $p = 0.24$). As an example of a protein which demonstrated no difference between control and PHH samples in the tandem MAF proteomics analysis, Western blots were performed for NCAN. The findings of this analysis for NCAN confirmed that there were no differences among groups ($p = 0.8$; data not shown).

DISCUSSION

The current study was designed to evaluate the feasibility and reproducibility of tandem MAF-proteomics and to use the technique to identify potential diagnostic CSF markers of PHH. The results presented herein provide convincing evidence that CSF levels of protein mediators of neurodevelopment, such as L1CAM, APP, BCAN, and NCAM-1 are significantly elevated in PHH relative to control, and that they decrement toward control levels after initiation of PHH treatment. These CSF proteins warrant further investigation as potential diagnostic markers of PHH. Notably, however, the observation of alterations in the levels of protein mediators of neurodevelopment in the CSF of infants with PHH also is entirely novel. The late preterm period is a critical interval for neurodevelopment, and the relationship of the observed CSF protein increases to long-term developmental disability remains unclear at present. Further study will be required to elucidate any possible association.

Proteomics analysis of PHH cerebrospinal fluid—or any CSF in preterm infants—has not previously been reported.

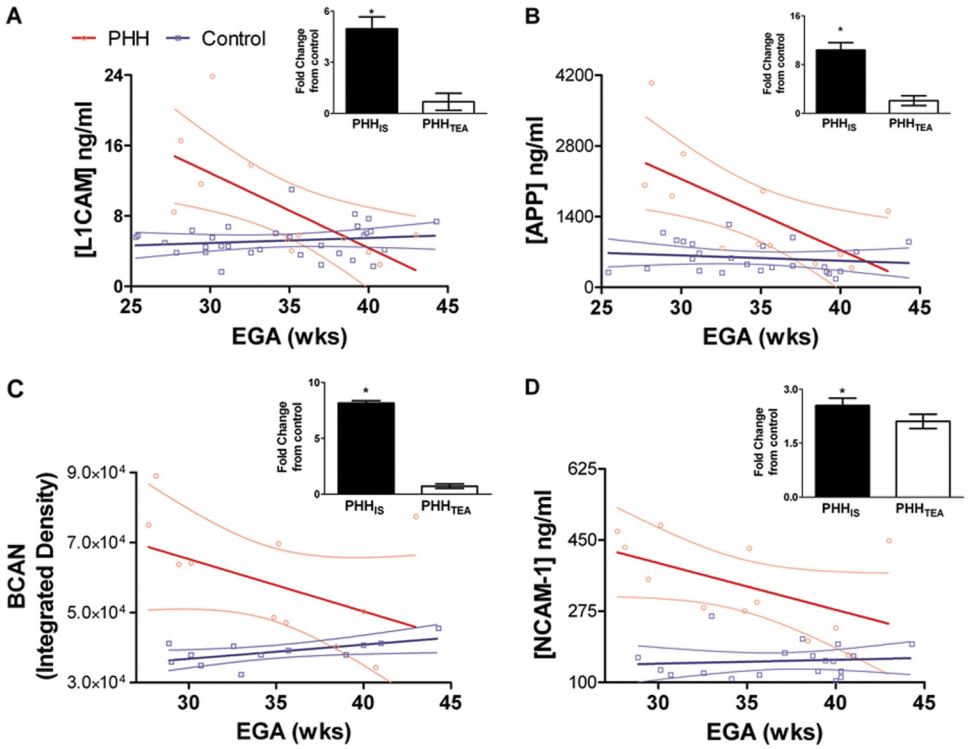

FIG. 6. **The CSF levels of several key protein mediators of neurodevelopment are elevated in PHH but return to control levels after initiation of PHH treatment.** *A–D*, (insets). Using tandem MAF-proteomics, CSF from the initial PHH sample (PHH_{IS}) demonstrated 4.96, 10.4, 8.17, and 2.55 fold increase in L1CAM, APP, BCAN, and NCAM-1 over control CSF, respectively. At TEA, there was no significant difference detected when comparing PHH (PHH_{TEA}) with control for three of the aforementioned proteins; NCAM-1 was decreasing, but at a slower rate and therefore was still different between PHH and control groups ($p = 0.02$). $n = 3$ for each group in the tandem MAF proteomics data. *A–D*, Graphs plotting protein levels *versus* EGA in weeks are shown. ELISAs for L1CAM (PHH: $n = 12$; control: $n = 31$), APP (PHH: $n = 12$; control: $n = 25$), and NCAM-1 (PHH: $n = 12$; control: $n = 19$), and a Western blot for BCAN (PHH: $n = 12$; control: $n = 12$), verified the increases in CSF levels of these proteins observed in PHH infants compared with age-matched controls. There was variability in the time course of return to control levels for these proteins, such that the increase in L1CAM appeared to resolve earlier than NCAM-1. The color red denotes the PHH group and the color blue was used for the control group. The thick solid lines are the best fit regression lines with 95% confidence interval boundaries (thinner lines).

PHH CSF by nature is replete with proteins derived from blood and inflammatory processes. In order to permit analysis of low abundance proteins, we applied the method of tandem MAF to prepare samples for label-free quantitative proteomics analysis. Multi-affinity fractionation has been previously used in protein biomarker discovery studies using a variety of methods and affinity media (reviewed in (40)). For the analysis of quantity-limited clinical samples, we incorporated an automated MAF method into our nano-LC-MS based proteomics platform. The method uses two types of multi-affinity stationary phase, one for capturing 14 of the most abundant proteins in plasma and a second column that retains plasma proteins of medium abundance (14). By using this approach we were able to minimize sample loss, increase fractionation reproducibility, and perform quantitative analysis of PHH CSF proteins from limited clinical samples that were procured during the course of treatment. During the discovery phase, we quantified a large set of proteins that have been associated with neural development and have been detected in the proteomic analysis of a cortical neuron secretome (41).

From our discovery studies of longitudinally procured samples throughout clinical treatment, we verified the promising biomarkers of clinical response, L1CAM, APP, BCAN, and NCAM-1 using immunometric methods (*e.g.* ELISAs and Westerns). These results verified our proteomic approach to analyzing CSF and introduced the potential that these proteins have with respect to clinical utility.

Presently, there is no consensus regarding the treatment of PHH. Clinical trials are needed to generate guidelines for the timing of ventricular decompression and selection of neurosurgical technique, but these efforts have been hindered by a dearth of quantifiable metrics for use in directing intervention or providing feedback regarding treatment efficacy. Physical findings such as head circumference, tenseness of the anterior fontanel, and splaying of cranial sutures are crude parameters, and changes in vital signs occur only very late in the disease course. Because the physical findings of PHH in the preterm infant are unreliable, image-based ventricular size measurements have become the primary guide for PHH treatment, but these may be affected by neurological injury (IVH, infarct, hypoxia-ischemia, encephalopathy of prematurity), at-

rophy, white matter volume loss, and impaired brain development—all of which are common in preterm infants. To advance this field and improve outcomes in preterm infants with PHH, developing new tools to complement ventricular measures is critical. CSF biomarkers of PHH or PHH-related adverse neurological outcomes such as those proposed herein would be most immediately useful in clinical trials for PHH, but ultimately would be applied to clinical practice.

Although the technical adaptations employed in this study and their application to preterm infant CSF are novel, the findings described herein, particularly those regarding the observed elevations in the key proteins known to mediate neurodevelopment, L1CAM, APP, BCAN, NCAM-1, and others are of particular importance. Prior to the current study, the majority of research in PHH has revolved around inflammatory mediators and nonspecific markers of tissue injury. The CSF levels of protein mediators of neurodevelopment have not been previously investigated in PHH. Importantly, very preterm birth and PHH occur during a critical gestational interval, from 24–40 weeks EGA, during which key neurodevelopmental events are occurring. The generation of neural networks, synaptogenesis, precursor cell migration, and cortical development and folding are all occurring during this interval. Disruption of these normal events, coupled with injurious stimuli, may have significant and long-lasting implications for the brain developing under these pathological conditions.

In the current study, L1CAM, APP, and BCAN were selected for confirmatory studies because of: (1) their observed effect size (5.0-, 10.4-, and 8.2-fold change from control levels for L1CAM, APP, and BCAN respectively); (2) well-characterized roles in multiple neurodevelopmental processes; and (3) potential for pathological sequelae with aberrant regulation. L1CAM is a type I membrane glycoprotein that is critically involved in axonal guidance, neuronal migration, myelination, and structural brain development (42, 43). Mutations in the L1CAM gene cause hydrocephalus and disabling cognitive deficits (44–47). However, abnormally high L1CAM levels also may contribute to morphological anomalies and functional deficits (48–50). APP is also a type I membrane protein with involvement in cell adhesion (51), synaptogenesis (52), and neural precursor cell proliferation (53). Although normal levels of APP are required for learning and memory (54), excess levels may be more likely to result in pathological accumulations of amyloid-β, which have been widely implicated in neurodegeneration and the cognitive effects of Alzheimer's disease. BCAN is a developmentally regulated extracellular matrix chondroitin sulfate proteoglycan that has been shown to regulate the synapse formation and maintenance (55). Further, in excess quantities, this protein appears to be an important contributor to the glial scarring that follows newborn brain injuries such as hypoxia-ischemia (25). Thus, because of their dual roles in neurodevelopmental processes and in hydrocephalus, cognitive disability, and newborn brain injury, L1CAM, APP, and BCAN are natural choices for candidate markers of PHH.

The results presented in this study showed not only sustained increases the CSF levels of select protein mediators of neurodevelopment, but also that these increases resolved over a protein-specific time course. In the four primary proteins studied over preterm interval (L1CAM, APP, BCAN, and NCAM-1), there was considerable variability in the time course of recovery toward control levels. For the purposes of this study, return to control levels was defined as that time point where the 95% confidence intervals for PHH and control intersected (Fig. 6). Thus, for L1CAM, PHH levels were considered to be at control values by 35 weeks EGA. Conversely, PHH NCAM-1 levels did not appear to reach control values until ~40 weeks EGA. Although these data are limited by sample size and data dispersion, it is of significant interest to fully elucidate these time courses, as they may impact long-term neurodevelopment.

The origin of the observed increases in L1CAM, APP, BCAN, NCAM-1, and other proteins is unclear at present. Potential sources of these protein elevations include rupture of the ependymal surface (from IVH), release from ventriculomegaly induced parenchymal stretch, cleavage of native protein, sequelae from hemorrhage or inflammation, or from the IVH itself. Although the clinical design of the current study presents limitations in our ability to speculate on the source of the proteins, we can utilize the work of Schutzer *et al.* (11) and others to provide insight into this issue. Schutzer *et al.* used IgY-14 LC-MS to compare proteins in the CSF of adult humans to those observed in plasma from a cohort of trauma patients and found a large percentage (56%) of proteins that appeared to be present only in CSF. Among those proteins identified exclusively or preferentially in CSF were BCAN, NCAN, VGF, SCG2, SEZ6, NRXN, and BASP1 (11), all of which were present in the tandem MAF proteomics analysis of the preterm CSF in the current study. Moreover, we have verified BCAN, NCAN, VGF, and SCG2 with Western analysis. Certainly, many of the proteins that we observed were of plasma origin (*e.g.* ApoA2 and ApoA4) or could have had more than one source (*e.g.* ACTB, MMP9, APP), but the observation of selective increases in brain or CSF-specific proteins (*e.g.* BCAN) provides evidence implicating ependymal rupture, neural injury, or parenchymal stretch as the source of at least some of the observed proteins.

It is tempting to surmise that profound changes in the levels of these and other proteins known to regulate cell-cell adhesion, synaptogenesis, myelination, and precursor cell migration could result in long-lasting structural and functional neurological deficits. Of particular interest will be further delineating the extent and extension of these proteins; for example, could transudative migration and/or accumulation of these proteins in the periventricular region contribute to periventricular white matter injury?

The CSF used in the current study was acquired from human preterm infants, and all samples were obtained only as clinical indicated. Although we have proposed a potential pathophysiological relationship between elevations of specific CSF proteins and PHH-related neurological impairment, possible mechanisms responsible cannot be delineated with the available data. The PHH CSF used in this study was acquired from a total 10 subjects. All ten required VP shunts. One subject expired because of nonneurological causes, and the other nine developed both cognitive and motor disabilities, with eight of nine diagnosed with cerebral palsy. Formal neurodevelopmental testing scoring was only available for three of the nine. Clearly, these data are inadequate to ascertain the relationship of CSF L1CAM, APP, BCAN, and NCAM-1 to VP shunt requirement or neurodevelopmental outcome; however, these parameters are the subject of an ongoing multi-institutional prospective clinical study in which CSF from each subject is banked in a CSF repository. With prospectively-acquired clinical, radiographic, surgical, and neurobehavioral data, we will fully characterize the relationship of these CSF proteins to surgical and neurodevelopmental outcomes.

Our results demonstrate the utility and validity of tandem MAF proteomics in the study of neurological conditions such as PHH. Further, despite a small sample size, this powerful technique enabled us to identify several novel candidate markers of PHH, L1CAM, APP, BCAN, and NCAM-1, which will be further investigated for their clinical diagnostic utility and their relationship to PHH-related neurological disability.

Acknowledgments—We thank Alan Davis and Petra Erdmann-Gilmore for exceptional technical assistance for highly reproducible MAF, peptide preparation, and nano-LC-MS. We also thank Dr. Michael Wallendorf for expert statistical assistance and Dr. Richard LeDuc for helpful discussions during the planning of the proteomics experiments. DanteR was written by Tom Taverner Thomas. Taverner@pnl.gov and Ashoka Polpitiya for the U.S. Department of Energy (PNNL, Richland, WA). Website: http://omics.pnl.gov/software. This computer software was prepared by Battelle Memorial Institute, hereinafter the Contractor, under Contract No. DE-AC05–76RL0 1830 with the Department of Energy (DOE). All rights in the computer software are reserved by DOE on behalf of the United States Government and the Contractor as provided in the Contract.

* This research was supported with grants P41RR000954 and UL1 RR024992 from the National Center for Research Resources, a component of the National Institutes of Health (NIH) and NIH Roadmap for Medical Research. Dr. Limbrick received support from the Children's Surgical Sciences Institute, a Just-in-Time grant from the Institute for Clinical and Translational Sciences at Washington University, and the Department of Neurological Surgery at Washington University. Dr. Inder received support from the Doris Duke Charitable Foundation.

S This article contains supplemental Figs. S1 to S12 and Tables S1 to S5.

** To whom correspondence should be addressed: Department of Neurological Surgery, Washington University School of Medicine, 660 South Euclid Ave., Campus Box 8057, St. Louis, MO 63110. Tel.: (314)362-8375; Fax: (314)454-2818; E-mail: moralesd@wudosis.wustl.edu.

REFERENCES

1. Volpe, J. J. (2008) *Neurology of the newborn*, Elsevier, Philadelphia
2. Adams-Chapman, I., Hansen, N. I., Stoll, B. J., and Higgins, R. (2008) Neurodevelopmental outcome of extremely low birth weight infants with posthemorrhagic hydrocephalus requiring shunt insertion. *Pediatrics* **121,** e1167–1177
3. Smyser, C. D., Inder, T. E., Shimony, J. S., Hill, J. E., Degnan, A. J., Snyder, A. Z., and Neil, J. J. (2010) Longitudinal analysis of neural network development in preterm infants. *Cereb Cortex.* **12,** 2852–2862
4. Miyan, J. A., Zendah, M., Mashayekhi, F., and Owen-Lynch, P. J. (2006) Cerebrospinal fluid supports viability and proliferation of cortical cells in vitro, mirroring in vivo development. *Cerebrospinal Fluid Res* **3,** 2
5. Lehtinen, M. K., Zappaterra, M. W., Chen, X., Yang, Y. J., Hill, A. D., Lun, M., Maynard, T., Gonzalez, D., Kim, S., Ye, P., D'Ercole, A. J., Wong, E. T., LaMantia, A. S., and Walsh, C. A. (2011) The cerebrospinal fluid provides a proliferative niche for neural progenitor cells. *Neuron* **69,** 893–905
6. Waybright, T., Avellino, A. M., Ellenbogen, R. G., Hollinger, B. J., Veenstra, T. D., and Morrison, R. S. (2010) Characterization of the human ventricular cerebrospinal fluid proteome obtained from hydrocephalic patients. *J. Proteomics* **73,** 1156–1162
7. Anderson, N. L., and Anderson, N. G. (2002) The human plasma proteome: history, character, and diagnostic prospects. *Mol. Cell. Proteomics* **1,** 845–867
8. Linke, T., Doraiswamy, S., and Harrison, E. H. (2007) Rat plasma proteomics: effects of abundant protein depletion on proteomic analysis. *J. Chromatogr. B Analyt. Technol. Biomed. Life Sci.* **849,** 273–281
9. Roche, S., Delorme, B., Oostendorp, R. A., Barbet, R., Caton, D., Noel, D., Boumediene, K., Papadaki, H. A., Cousin, B., Crozet, C., Milhavet, O., Casteilla, L., Hatzfeld, J., Jorgensen, C., Charbord, P., and Lehmann, S. (2009) Comparative proteomic analysis of human mesenchymal and embryonic stem cells: towards the definition of a mesenchymal stem cell proteomic signature. *Proteomics* **9,** 223–232
10. Pieper, R., Gatlin, C. L., Makusky, A. J., Russo, P. S., Schatz, C. R., Miller, S. S., Su, Q., McGrath, A. M., Estock, M. A., Parmar, P. P., Zhao, M., Huang, S. T., Zhou, J., Wang, F., Esquer-Blasco, R., Anderson, N. L., Taylor, J., and Steiner, S. (2003) The human serum proteome: display of nearly 3700 chromatographically separated protein spots on two-dimensional electrophoresis gels and identification of 325 distinct proteins. *Proteomics* **3,** 1345–1364
11. Schutzer, S. E., Liu, T., Natelson, B. H., Angel, T. E., Schepmoes, A. A., Purvine, S. O., Hixson, K. K., Lipton, M. S., Camp, D. G., Coyle, P. K., Smith, R. D., and Bergquist, J. (2010) Establishing the proteome of normal human cerebrospinal fluid. *PLoS One* **5,** e10980
12. Maccarrone, G., Milfay, D., Birg, I., Rosenhagen, M., Holsboer, F., Grimm, R., Bailey, J., Zolotarjova, N., and Turck, C. W. (2004) Mining the human cerebrospinal fluid proteome by immunodepletion and shotgun mass spectrometry. *Electrophoresis* **25,** 2402–2412
13. Huang, L., Harvie, G., Feitelson, J. S., Gramatikoff, K., Herold, D. A., Allen, D. L., Amunngama, R., Hagler, R. A., Pisano, M. R., Zhang, W. W., and Fang, X. (2005) Immunoaffinity separation of plasma proteins by IgY microbeads: meeting the needs of proteomic sample preparation and analysis. *Proteomics* **5,** 3314–3328
14. Qian, W. J., Kaleta, D. T., Petritis, B. O., Jiang, H., Liu, T., Zhang, X., Mottaz, H. M., Varnum, S. M., Camp, D. G., 2nd, Huang, L., Fang, X., Zhang, W. W., and Smith, R. D. (2008) Enhanced detection of low abundance human plasma proteins using a tandem IgY12-SuperMix immunoaffinity separation strategy. *Mol. Cell. Proteomics* **7,** 1963–1973
15. King, J. B., Gross, J., Lovly, C. M., Rohrs, H., Piwnica-Worms, H., and Townsend, R. R. (2006) Accurate mass-driven analysis for the characterization of protein phosphorylation. Study of the human Chk2 protein kinase. *Anal. Chem.* **78,** 2171–2181
16. Keller, A., Nesvizhskii, A. I., Kolker, E., and Aebersold, R. (2002) Empirical statistical model to estimate the accuracy of peptide identifications made by MS/MS and database search. *Anal. Chem.* **74,** 5383–5392
17. Neubert, H., Bonnert, T. P., Rumpel, K., Hunt, B. T., Henle, E. S., and James, I. T. (2008) Label-free detection of differential protein expression by LC/MALDI mass spectrometry. *J. Proteome Res.* **7,** 2270–2279
18. Polpitiya, A. D., Qian, W. J., Jaitly, N., Petyuk, V. A., Adkins, J. N., Camp, D. G., 2nd, Anderson, G. A., and Smith, R. D. (2008) DAnTE: a statistical tool for quantitative analysis of -omics data. *Bioinformatics* **24,** 1556–1558

19. Karpievitch, Y., Stanley, J., Taverner, T., Huang, J., Adkins, J. N., Ansong, C., Heffron, F., Metz, T. O., Qian, W. J., Yoon, H., Smith, R. D., and Dabney, A. R. (2009) A statistical framework for protein quantitation in bottom-up MS-based proteomics. *Bioinformatics* **25,** 2028–2034
20. Brümmendorf, T., Kenwrick, S., and Rathjen, F. G. (1998) Neural cell recognition molecule L1: from cell biology to human hereditary brain malformations. *Curr. Opin. Neurobiol.* **8,** 87–97
21. Maness, P. F., and Schachner, M. (2007) Neural recognition molecules of the immunoglobulin superfamily: signaling transducers of axon guidance and neuronal migration. *Nat. Neurosci.* **10,** 19–26
22. Gralle, M., and Ferreira, S. T. (2007) Structure and functions of the human amyloid precursor protein: the whole is more than the sum of its parts. *Prog. Neurobiol.* **82,** 11–32
23. Araki, Y., Tomita, S., Yamaguchi, H., Miyagi, N., Sumioka, A., Kirino, Y., and Suzuki, T. (2003) Novel cadherin-related membrane proteins, Alcadeins, enhance the X11-like protein-mediated stabilization of amyloid beta-protein precursor metabolism. *J. Biol. Chem.* **278,** 49448–49458
24. Hintsch, G., Zurlinden, A., Meskenaite, V., Steuble, M., Fink-Widmer, K., Kinter, J., and Sonderegger, P. (2002) The calsyntenins–a family of postsynaptic membrane proteins with distinct neuronal expression patterns. *Mol. Cell. Neurosci.* **21,** 393–409
25. Leonardo, C. C., Eakin, A. K., Ajmo, J. M., and Gottschall, P. E. (2008) Versican and brevican are expressed with distinct pathology in neonatal hypoxic-ischemic injury. *J. Neurosci. Res.* **86,** 1106–1114
26. Ortega, N., Behonick, D., Stickens, D., and Werb, Z. (2003) How proteases regulate bone morphogenesis. *Ann. N.Y. Acad. Sci.* **995,** 109–116
27. Letourneau, P. C. (2009) Actin in axons: stable scaffolds and dynamic filaments. *Results Probl. Cell. Differ.* **48,** 65–90
28. Sekino, Y., Kojima, N., and Shirao, T. (2007) Role of actin cytoskeleton in dendritic spine morphogenesis. *Neurochem. Int.* **51,** 92–104
29. Bunnell, T. M., and Ervasti, J. M. (2010) Delayed embryonic development and impaired cell growth and survival in Actg1 null mice. *Cytoskeleton* **67,** 564–572
30. Border, B. G., Lin, S. C., Griffin, W. S., Pardue, S., and Morrison-Bogorad, M. (1993) Alterations in actin-binding beta-thymosin expression accompany neuronal differentiation and migration in rat cerebellum. *J. Neurochem.* **61,** 2104–2114
31. Yin, H. L. (1987) Gelsolin: calcium- and polyphosphoinositide-regulated actin-modulating protein. *Bioessays* **7,** 176–179
32. Rozek, W., Ricardo-Dukelow, M., Holloway, S., Gendelman, H. E., Wojna, V., Melendez, L. M., and Ciborowski, P. (2007) Cerebrospinal fluid proteomic profiling of HIV-1-infected patients with cognitive impairment. *J. Proteome Res.* **6,** 4189–4199
33. Kulakowska, A., Drozdowski, W., Sadzynski, A., Bucki, R., and Janmey, P. A. (2008) Gelsolin concentration in cerebrospinal fluid from patients with multiple sclerosis and other neurological disorders. *Eur. J. Neurol.* **15,** 584–588
34. Ji, L., Chauhan, A., Wegiel, J., Essa, M. M., and Chauhan, V. (2009) Gelsolin is proteolytically cleaved in the brains of individuals with Alzheimer's disease. *J. Alzheimers Dis.* **18,** 105–111
35. Becerra, S. P., Palmer, I., Kumar, A., Steele, F., Shiloach, J., Notario, V., and Chader, G. J. (1993) Overexpression of fetal human pigment epithelium-derived factor in Escherichia coli. A functionally active neurotrophic factor. *J. Biol. Chem.* **268,** 23148–23156
36. Becerra, S. P., Sagasti, A., Spinella, P., and Notario, V. (1995) Pigment epithelium-derived factor behaves like a noninhibitory serpin. Neurotrophic activity does not require the serpin reactive loop. *J. Biol. Chem.* **270,** 25992–25999
37. Oberg, A. L., and Vitek, O. (2009) Statistical design of quantitative mass spectrometry-based proteomic experiments. *J. Proteome Res.* **8,** 2144–2156
38. Ciborowski, P., Kadiu, I., Rozek, W., Smith, L., Bernhardt, K., Fladseth, M., Ricardo-Dukelow, M., and Gendelman, H. E. (2007) Investigating the human immunodeficiency virus type 1-infected monocyte-derived macrophage secretome. *Virology* **363,** 198–209
39. Paolucci, S., Antonucci, G., Grasso, M. G., Morelli, D., Troisi, E., Coiro, P., De Angelis, D., Rizzi, F., and Bragoni, M. (2001) Poststroke depression, antidepressant treatment and rehabilitation results. A case-control study. *Cerebrovasc Dis.* **12,** 264–271
40. Wetterhall, M., Zuberovic, A., Hanrieder, J., and Bergquist, J. (2010) Assessment of the partitioning capacity of high abundant proteins in human cerebrospinal fluid using affinity and immunoaffinity subtraction spin columns. *J. Chromatogr. B Analyt. Technol. Biomed. Life Sci.* **878,** 1519–1530
41. Thouvenot, E., Urbach, S., Dantec, C., Poncet, J., Séveno, M., Demettre, E., Jouin, P., Touchon, J., Bockaert, J., and Marin, P. (2008) Enhanced detection of CNS cell secretome in plasma protein-depleted cerebrospinal fluid. *J. Proteome Res.* **7,** 4409–4421
42. Schachner, M. (1997) Neural recognition molecules and synaptic plasticity. *Curr. Opin. Cell Biol.* **9,** 627–634
43. Mechtersheimer, S., Gutwein, P., Agmon-Levin, N., Stoeck, A., Oleszewski, M., Riedle, S., Postina, R., Fahrenholz, F., Fogel, M., Lemmon, V., and Altevogt, P. (2001) Ectodomain shedding of L1 adhesion molecule promotes cell migration by autocrine binding to integrins. *J. Cell Biol.* **155,** 661–673
44. Yamasaki, M., Thompson, P., and Lemmon, V. (1997) CRASH syndrome: mutations in L1CAM correlate with severity of the disease. *Neuropediatrics* **28,** 175–178
45. Weller, S., and Gärtner, J. (2001) Genetic and clinical aspects of X-linked hydrocephalus (L1 disease): Mutations in the L1CAM gene. *Hum. Mutat.* **18,** 1–12
46. Halliday, J., Chow, C. W., Wallace, D., and Danks, D. M. (1986) X linked hydrocephalus: a survey of a 20 year period in Victoria, Australia. *J. Med. Genet.* **23,** 23–31
47. Fransen, E., Van Camp, G., D'Hooge, R., Vits, L., and Willems, P. J. (1998) Genotype-phenotype correlation in L1 associated diseases. *J. Med. Genet.* **35,** 399–404
48. Poltorak, M., Khoja, I., Hemperly, J. J., Williams, J. R., el-Mallakh, R., and Freed, W. J. (1995) Disturbances in cell recognition molecules (N-CAM and L1 antigen) in the CSF of patients with schizophrenia. *Exp. Neurol.* **131,** 266–272
49. Haspel, J., and Grumet, M. (2003) The L1CAM extracellular region: a multi-domain protein with modular and cooperative binding modes. *Front Biosci.* **8,** s1210–1225
50. Maretzky, T., Schulte, M., Ludwig, A., Rose-John, S., Blobel, C., Hartmann, D., Altevogt, P., Saftig, P., and Reiss, K. (2005) L1 is sequentially processed by two differently activated metalloproteases and presenilin/gamma-secretase and regulates neural cell adhesion, cell migration, and neurite outgrowth. *Mol. Cell. Biol.* **25,** 9040–9053
51. Narindrasorasak, S., Lowery, D. E., Altman, R. A., Gonzalez-DeWhitt, P. A., Greenberg, B. D., and Kisilevsky, R. (1992) Characterization of high affinity binding between laminin and Alzheimer's disease amyloid precursor proteins. *Lab. Invest.* **67,** 643–652
52. Mucke, L., Masliah, E., Johnson, W. B., Ruppe, M. D., Alford, M., Rockenstein, E. M., Forss-Petter, S., Pietropaolo, M., Mallory, M., and Abraham, C. R. (1994) Synaptotrophic effects of human amyloid beta protein precursors in the cortex of transgenic mice. *Brain Res.* **666,** 151–167
53. Caillé, I., Allinquant, B., Dupont, E., Bouillot, C., Langer, A., Müller, U., and Prochiantz, A. (2004) Soluble form of amyloid precursor protein regulates proliferation of progenitors in the adult subventricular zone. *Development* **131,** 2173–2181
54. Ring, S., Weyer, S. W., Kilian, S. B., Waldron, E., Pietrzik, C. U., Filippov, M. A., Herms, J., Buchholz, C., Eckman, C. B., Korte, M., Wolfer, D. P., and Müller, U. C. (2007) The secreted beta-amyloid precursor protein ectodomain APPs alpha is sufficient to rescue the anatomical, behavioral, and electrophysiological abnormalities of APP-deficient mice. *J. Neurosci.* **27,** 7817–7826
55. Pyka, M., Wetzel, C., Aguado, A., Geissler, M., Hatt, H., and Faissner, A. (2011) Chondroitin sulfate proteoglycans regulate astrocyte-dependent synaptogenesis and modulate synaptic activity in primary embryonic hippocampal neurons. *Eur. J. Neurosci.* **33,** 2187–2202
56. Perkins, D. N., Pappin, D. J., Creasy, D. M., and Cottrell, J. S. (1999) Probability-based protein identification by searching sequence databases using mass spectrometry data. *Electrophoresis* **20,** 3551–3567
57. Roche, S. L., O'Sullivan, J. J., and Kantor, P. F. (2010) Hypertension after pediatric cardiac transplantation: detection, etiology, implications and management. *Pediatr. Transplant* **14,** 159–168
58. Keilhauer, G., Faissner, A., and Schachner, M. (1985) Differential inhibition of neurone-neurone, neurone-astrocyte and astrocyte-astrocyte adhesion by L1, L2 and N-CAM antibodies. *Nature* **316,** 728–730